THE JOURNAL OF PHYSICAL CHEMISTRY C
A JOURNAL OF THE AMERICAN CHEMICAL SOCIETY

pubs.acs.org/JPCC

Article

Thermodynamic, Thermal, and Structural Stability of Bimetallic MIL-53 ($Al_{1-x}Cr_x$)

Published as part of The Journal of Physical Chemistry virtual special issue "Alexander Boldyrev Festschrift".

Esra Y. Mertsoy, Xianghui Zhang, Cody B. Cockreham, Vitaliy G. Goncharov, Xiaofeng Guo,* Jun Wang, Nian Wei, Hui Sun, and Di Wu*

Cite This: *J. Phys. Chem. C* 2021, 125, 14039−14047

Read Online

ACCESS | Metrics & More | Article Recommendations | Supporting Information

ABSTRACT: Understanding the stability of porous materials, especially metal−organic frameworks (MOFs), is central to defining their applications in gas storage, separation, and catalysis. Herein, integrating high-temperature drop combustion calorimetry as well as simultaneous thermal and *in situ* structural analyses, we performed a comprehensive study on the thermodynamic, thermal, and structural stabilities of MOF in air. A family of MIL-53 ($Al_{1-x}Cr_x$) with systematically tuned metal contents was intentionally chosen considering their unique property that H_2BDC species serve as both coordinated linkers and guest species confined. The results suggest that as temperature increases, all samples underwent (1) a phase transition from the pore-filled *Pnma* to the *Imma* with empty pores, (2) structural degradation, and (3) complete oxidation (burning). At the same temperature, as the chromium (Cr) content increases, the thermal and structural stability of MIL-53 ($Al_{1-x}Cr_x$) in air decreases. In contrast, interestingly, the intrinsic thermodynamic stability systematically increases as a function of Cr content, evidenced by the more exothermic enthalpies of formation, ranging from 92.8 ± 73.4 kJ/mol (slightly metastable) to −1593.2 ± 60.8 kJ/mol (stable). Such a phenomenon is likely due to enhanced H_2BDC−MIL-53 guest−host interactions upon Cr substitution, which energetically neutralize the metastability of MIL-53 open frameworks. This study highlights that the thermal, structural, and energetic stabilities are different and have equal importance in governing the synthesis and applications of MOFs.

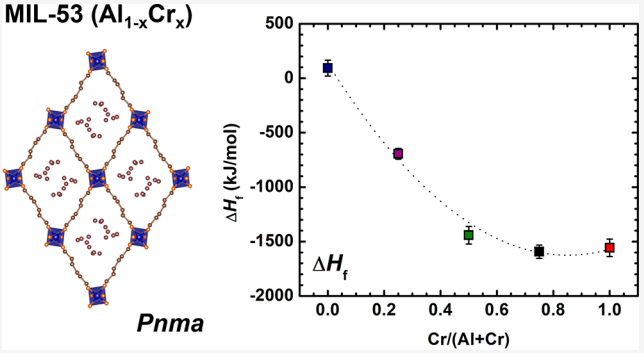

INTRODUCTION

Metal−organic frameworks (MOFs) are solid-state "molecular tinker toy like" crystalline porous materials constructed by self-assembly of metal nodes and organic linkers into multidimensional lattices through coordination chemistry.[1,2] Compared to traditional inorganic porous materials, such as zeolites, mesoporous silica, and carbon polymorphs, the distinct advantage of MOFs is their intrinsic modifiability in metal nodes, functional linkers, and exchangeable building blocks, which leads to promising application potential in gas storage,[3] adsorption and separation,[4−7] catalysis,[8−11] drug delivery, and molecular sensing.[12−14] Numerous topologies have been synthesized, whereas large-scale industrial applications of MOFs are hindered by their stability issues at elevated temperature, under humid environments, and within harsh chemicals. Extensive research has been performed on the synthesis, structure, and performance evaluation of MOFs. However, much fewer studies have been conducted on systematic investigation into MOF stability, which is the major hurdle to overcome prior to their eventual applications.

The experimental thermodynamic studies on formation stability and energetic landscape of MOFs were pioneered by Navrotsky and colleagues, in which near-room-temperature solution calorimetry with different solvents, including acid, base, and organic solvents, was employed to quantify the enthalpies of formation of MOFs with different porosity, structure, and polymorphism.[15−20] Parallelly, Woodfield's group designed a highly customized setup for the first set of low-temperature heat capacity measurements on MOFs to elucidate their entropic evolutions as a function of temperature.[21] These studies suggest that the magnitude and trend of macroscopic thermodynamic properties, such as formation enthalpy and heat capacity, reflect subtle variations in the

Received: March 23, 2021
Revised: May 21, 2021
Published: June 22, 2021

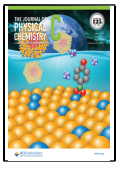

https://doi.org/10.1021/acs.jpcc.1c02623
J. Phys. Chem. C 2021, 125, 14039−14047

microscopic compositional and structural factors of MOFs. Generally, MOFs are less stable and less exothermic or even endothermic compared with their corresponding dense phase assemblages. It is also indicated that there appears to be not much thermodynamic penalty for the synthesis of MOF structures with ultrahigh porosity and specific surface area, and the energetic stabilities among MOF polymorphs are not significantly different. Moreover, it was found that strong adsorbate−MOF guest−host interactions effectively stabilize MOFs in the synthesis processes and during applications involved in adsorption and separation. Recently, we reviewed these studies in detail,[22−24] in which the energetic landscape, entropy evolution as a function of temperature, and thermodynamics of molecule−materials interactions were summarized and discussed. These thermodynamic studies significantly enhanced our fundamental understanding on the intrinsic stability of MOF formation, yet we realized the lack of integrated *in situ* studies on the thermal, structural, and energetic (thermodynamic) stability on MOFs sharing the same topology with systematically tuned compositions.[22−24]

The objective of this study is to determine the energetic (thermodynamic), thermal, and structural stability of a group of MIL-53 in air as a function of temperature. MIL-53 ($Al_{1-x}Cr_x$) samples (M^{3+} = Al^{3+} or Cr^{3+}, $0 < x < 1$) were intentionally chosen to represent bimetallic MOFs with systematically tuned aluminum (Al) and chromium (Cr) contents. These MIL-53 ($Al_{1-x}Cr_x$) samples share a unique breathable framework structure with infinite chains of corner-sharing octahedra of Al^{3+} or Cr^{3+} coordinated with 1,4-benzenedicarboxylic acid (H_2BDC) linkers. The molar formula of as-synthesized MIL-53 ($Al_{1-x}Cr_x$) is denoted as M(OH)-(BDC)-$(H_2BDC)_x$, in which -$(H_2BDC)_x$ represents pore-confined H_2BDC molecules. The pore-filled phase of MIL-53 has a space group of *Pnma*, while its empty-pore structure belongs to *Imma* (see Figure 1). All samples were thoroughly

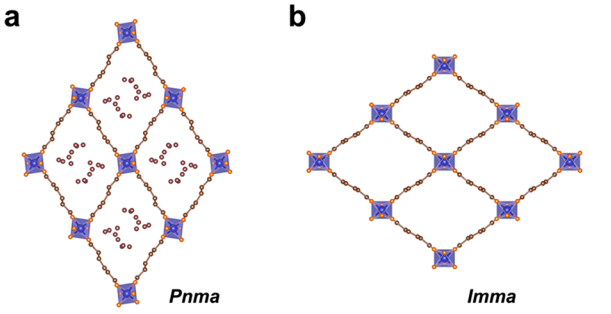

Figure 1. Schematic illustration of MIL-53 structures: (a) the pore-filled phase with *Pnma* space group and (b) the empty-pore phase with *Imma*.

investigated by *ex situ* and *in situ* powder X-ray diffraction (XRD), X-ray photoelectron spectroscopy (XPS), scanning electron microscopy (SEM), N_2 adsorption−desorption full isotherm analysis, and thermal analysis using an integrated thermogravimetry−differential scanning calorimetry−mass spectrometry (TG-DSC-MS) system. Subsequently, the formation enthalpies of MIL-53 ($Al_{1-x}Cr_x$) from dense phase assemblages of M_2O_3 and H_2BDC were determined by using high-temperature drop combustion calorimetry, which was recently developed to probe the formation energetics of organic and/or hybrid materials that cannot be dissolved at near-room temperature by traditional acid/base solutions and/or organic solvents.[25] This study reveals the complex relations among compositional factors that govern the thermal, structural, and energetic stabilities of MIL-53 ($Al_{1-x}Cr_x$).

EXPERIMENTAL METHODS

Materials Synthesis. Analytical grade aluminum nitrate nonahydrate [$Al(NO_3)_3{\cdot}9H_2O$], chromium nitrate nonahydrate [$Cr(NO_3)_3{\cdot}9H_2O$], terephthalic acid (H_2BDC), dimethylformamide (DMF), and methanol (MeOH) were purchased from Sigma-Aldrich. MIL-53 (Al) was-synthesized by using a method reported previously by Rallapalli et al.,[26] in which $Al(NO_3)_3{\cdot}9H_2O$, H_2BDC, and ultrapure water (1:0.5:80 molar ratio) were mixed under vigorous stirring and transferred to a 40 mL Teflon-lined stainless steel autoclave. After hydrothermal synthesis in an oven programmed at 220 °C for 72 h, the precipitate was collected and washed with ultrapure water (50 mL). Subsequently, the precipitate (∼1 g) was kept in 20 mL of DMF overnight to maximize the removal of unreacted BDC ligands. The product was further washed with 50 mL of MeOH to exchange the residual DMF followed by drying at 150 °C under vacuum for 12 h. MIL-53 (Cr) was synthesized according to the approach reported by Serre et al.[27] Specifically, $Cr(NO_3)_3{\cdot}9H_2O$, H_2BDC, and H_2O with a molar ratio of 1:1:280 were mixed under vigorous stirring and transferred to a Teflon-lined stainless steel autoclave for hydrothermal synthesis at 220 °C for 72 h. The relatively high synthesis temperature used in this study may lead to formation of bulk oxides outside of MOF pores, and postsynthesis centrifugation was applied to maximize the oxide removal.[28,29] The bimetallic MIL-53 ($Al_{1-x}Cr_x$) samples (x = 0.25, 0.5, and 0.75) were synthesized by using the same method as that of MIL-53 (Cr). The same purification and activation processes were used for all samples.

Standard Characterizations. We examined the morphology of each sample by scanning electron microscopy (SEM) using a Tescan Vega3 operated at 20 kV and 72 μA. *Ex situ* powder X-ray diffraction (XRD) experiments were performed by using a Rigaku SmartLab (Cu Kα radiation, λ = 1.5406 Å) operated at a scan rate of 4°/min in the 2θ range of 5°−80° for phase identification. X-ray photoelectron spectroscopy (XPS) measurements was performed with a Thermo Scientific K-Alpha spectrometer equipped with Al Kα (1486.6 eV) radiation. The surface area and pore dimension of each sample were measured by N_2 adsorption−desorption full isotherm analysis at 77 K on a Micromeritics 3Flex adsorption analyzer. Before each measurement, the sample was outgassed at 300 °C overnight. The specific surface area was calculated by using both the Langmuir ($S_{Langmuir}$) and the multiple-point Brunauer−Emmett−Teller (BET, S_{BET}) methods. The pore size and volume were calculated by using the Horvath−Kawazoe (HK) method.

Thermogravimetry−Differential Scanning Calorimetry−Mass Spectrometry (TG-DSC-MS). Thermal analyses with TG-DSC-MS were performed by using a STA 449 F3 Jupiter (Netzsch Instruments) coupled with a quadrupole mass spectrometer QMS 403 D (Aëolos).[30] In each analysis, about 5 mg sample was placed in a platinum (Pt) crucible heated from 35 to 700 °C at 10 °C/min under an air flow of 40 mL/min. The evolved gases were introduced through a heated transfer line (200 °C) and analyzed simultaneously by the MS. Signals recorded include m/z = 18 (H_2O), 32 (O_2), and 44 (CO_2). Moreover, we also took advantage of the TG-DSC-MS data for compositional analysis on all samples.

https://doi.org/10.1021/acs.jpcc.1c02623
J. Phys. Chem. C 2021, 125, 14039−14047

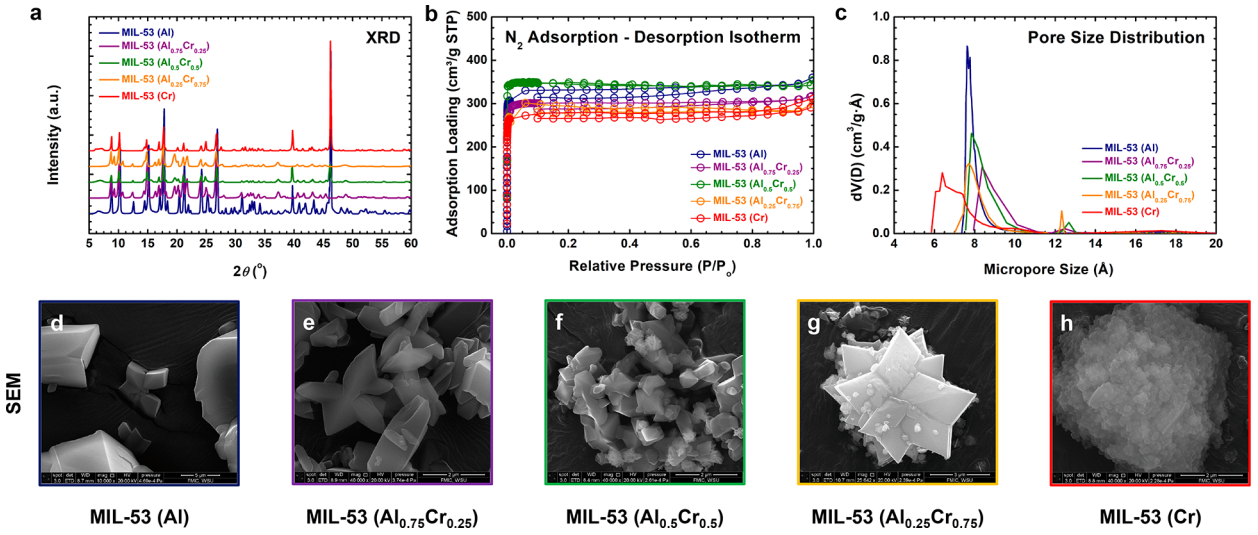

Figure 2. (a) *Ex situ* XRD patterns at room temperature, (b) N_2 adsorption−desorption full isotherms at 77 K, (c) pore size distribution, and (d−h) SEM images for all MIL-53 samples.

Table 1. Compositional and Surface Analysis Results on All MIL-53 Samples at 77 K

sample name	molecular formula	S_{BET} (m^2/g)	$S_{Langmuir}$ (m^2/g)	d_{HK} (Å)	$V_{HK\text{-micropore}}$ (cm^3/g)
MIL-53 (Al)	$(Al{-}OH)(C_8H_4O_4)(C_8H_6O_4)_{0.71}$	980.8	1495.3	7.8	0.5
MIL-53 ($Al_{0.75}Cr_{0.25}$)	$(Al_{0.74}Cr_{0.26}{-}OH)(C_8H_4O_4)(C_8H_6O_4)_{0.62}$	964.1	1340.8	7.5	0.5
MIL-53 ($Al_{0.5}Cr_{0.5}$)	$(Al_{0.52}Cr_{0.48}{-}OH)(C_8H_4O_4)(C_8H_6O_4)_{0.75}$	1095.2	1447.6	7.9	0.6
MIL-53 ($Al_{0.25}Cr_{0.75}$)	$(Al_{0.29}Cr_{0.71}{-}OH)(C_8H_4O_4)(C_8H_6O_4)_{0.60}$	905.0	1062.0	8.3	0.5
MIL-53 (Cr)	$(Cr{-}OH)(C_8H_4O_4)(C_8H_6O_4)_{0.49}$	890.1	1094.6	7.0	0.4

***In Situ* X-ray Diffraction (XRD).** Temperature-programmed *in situ* XRD data were obtained by using a Rigaku HT-1500 furnace on a platinum crucible,[31−34] with the platinum peaks removed by using software, with a heating rate of 10 °C/min under a 40 mL/min of air flow with an equilibrium time of 5 min by holding the target temperature prior to each scan. Using Bragg's law, we calculated the *d*-spacing of each sample. Lattice parameters in the *Pnma* (no. 62) space group were calculated by using (200), (020), and (202) peaks for *a*, *b*, and *c*, respectively. Lattice parameters for the *Imma* (no. 74) space group were calculated by using (101), (020), and (011) peaks for *a*, *b*, and *c*, respectively. Peaks were indexed by using crystal phase data reported by Loiseau et al.[35]

High-Temperature Drop Combustion Calorimetry. High-temperature combustion drop calorimetry measurements were conducted by using a Tian-Calvet twin microcalorimeter, Setaram Alexsys-1000, where the enthalpy of drop combustion (ΔH_{com}) of each sample was directly obtained.[25] Air-equilibrated MIL-53 ($Al_{1-x}Cr_x$) samples were pressed into cylindrical pellets between 4 and 6 mg. Each pellet was dropped from room temperature into an empty quartz crucible inside the reaction chamber kept at 800 °C. O_2 was continuously flushed through the chambers at a flowrate of 70 mL/min, providing a constant oxidative environment for the thermal combustion. The calibration factor of the instrument was determined by using benzoic acid ($C_6H_5CO_2H$). Prior to the calorimetric measurements, the samples were degassed at 150 °C for 12 h (10^{-7}−10^{-6} mmHg). We intentionally applied a low activation temperature of 150 °C for calorimetry experiments to keep the H_2BDC linkers confined within MIL-53 for investigation into the impacts of H_2BDC−MIL-53 guest−host interactions on energetic stability of materials. A 3D-printed calorimetric dropper was used to transfer and introduce the sample into the calorimeter to minimize exposure to the ambient environment.[36] At least three successful measurements were performed on each sample for deriving formation enthalpy (ΔH_f) and enthalpy of mixing (ΔH_{mix}).

RESULTS AND DISCUSSION

The *ex situ* XRD patterns at room temperature suggest that at room temperature all as-made samples belong to the orthorhombic *Pnma* space group corresponding to the phase with H_2BDC guest molecules confined, which is consistent with earlier studies (see Figure 2a).[27,35,37] N_2 adsorption−desorption isotherms at 77 K are plotted in Figure 2b. All samples present Type I isotherms, which strongly suggest microporosity. The specific surface areas were determined by using both BET and Langmuir methods. Specifically, MIL-53 ($Al_{0.5}Cr_{0.5}$) presents the highest BET surface area of 1095.2 m^2/g, while MIL-53 (Cr) has the lowest value of 890.1 m^2/g (see Table 1). The BET analysis results are in good agreement with previously reported values, ranging from 950 to 1500 m^2/g.[38−41] Langmuir surface analysis returns higher surface areas spanning between 1062.0 and 1495.3 m^2/g. The micropore volume of each sample was calculated by using the Horvath−Kawazoe (HK) method, ranging from 0.4 to 0.6 cm^3/g (see Table 1). Figure 2c also presents the pore size distributions of all samples. Generally, introduction of Cr broadens the pore size distribution of MIL-53.

The SEM images of all samples are presented in Figure 2d−h. MIL-53 (Al) shows star-shaped morphology with ordered octahedral crystals (~3.3 μm, see Figure 2d). This is consistent with observation in previous studies, in which star-shaped particles formed through intergrowth of orthorhombic MIL-53

https://doi.org/10.1021/acs.jpcc.1c02623
J. Phys. Chem. C 2021, 125, 14039−14047

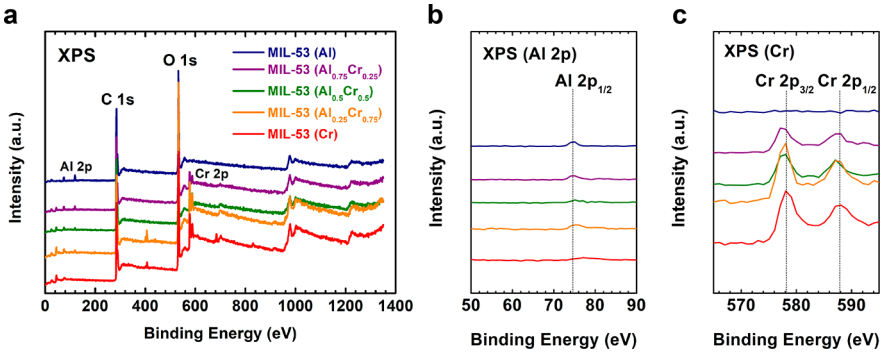

Figure 3. (a) XPS survey, (b) Al $2p_{1/2}$, and (c) Cr $2p_{1/2}$ and Cr $2p_{3/2}$ spectra of all MIL-53 samples.

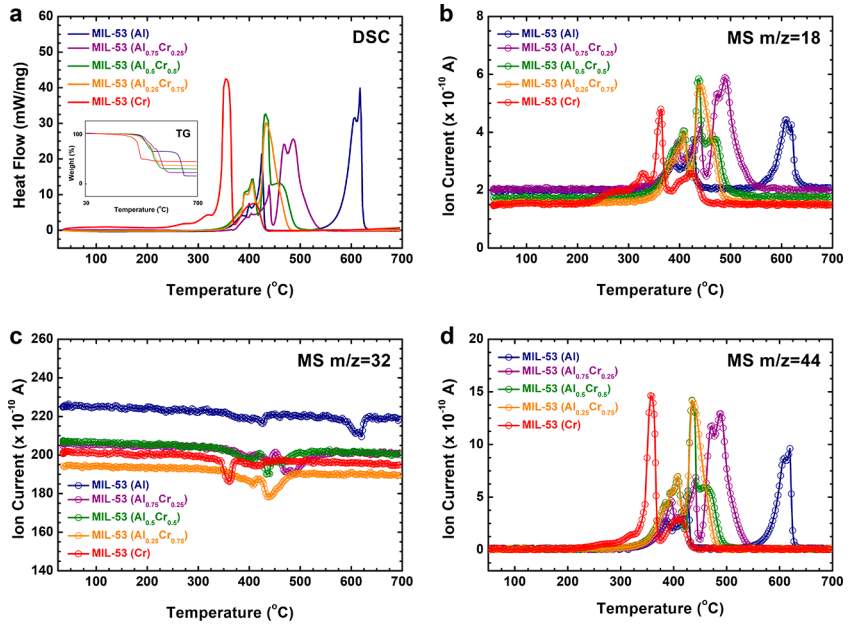

Figure 4. (a) DSC and TG (inset) profiles of all MIL-53 samples from 35 to 700 °C (10 °C/min) under air flow (50 mL/min). MS data of all MIL-53 samples: (b) H_2O, m/z = 18; (c) O_2, m/z = 32; and (d) CO_2, m/z = 44.

(Al) crystals.[42,43] As the Cr/Al ratio increases, morphology degradation and particle size decrease are observed (see Figure 2e–h). For MIL-53 (Cr), spherical particles (~150 nm) slightly smaller than previously reported sizes are seen (see Figure 2h).[44] Such particle size decrease is typical for MOFs synthesized in acid-free environments.[26−30] In short, the samples with higher Al content tend to present better morphology. Such morphological variations as a function of cation composition were also observed on other bimetallic MOFs.[45−49]

The XPS survey spectra with C 1s, O 1s, Cr 2p, and Al 2p peaks are presented in Figure 3a. The Al 2p and Cr 2p spectra are shown in Figures 3b and 3c, respectively. Specifically, the Al 2p3 and Al 2p1 are at 74.18−74.68 eV and 74.68−75.78 eV, respectively (see Figure 3a).[50] As the Cr content increases, the binding energies of Al 2p3 and Al 2p1 shift to higher values. For MIL-53 (Cr), the two prominent peaks at 577.68 and 587.18 eV are attributed to Cr $2p_{3/2}$ and Cr $2p_{1/2}$, respectively (see Figure 3c).[51,52] The remaining two peaks at 578.78 and 588.38 eV belong to Cr $2p_{3/2}$ and $2p_{1/2}$ satellite peaks, respectively. As the Cr/Al ratio increases, the prominent peaks slightly shift from 577.18 to 577.28 eV for Cr $2p_{3/2}$ and from 586.68 to 586.78 eV for Cr $2p_{1/2}$. Additionally, the intensity of Cr 2p increases as the Cr content increases, while the Al 2p presents weakening peaks—a clear indication of decrease in the number of Al cations (see Figure 3b,c). We also identified the metal compositions of all samples using XPS data (see Table 1), in which each sample presents an anticipated Al-to-Cr ratio. The deconvolution of each peak is presented in Figure S1 (Al) and Figure S2 (Cr).

Thermal Stability of MIL-53 ($Al_{1-x}Cr_x$) in Air. Thermal analysis using an integrated TG-DSC-MS system is employed to evaluate the thermal stability of MIL-53 ($Al_{1-x}Cr_x$) (see Figure 4a–d). The weight loss of MIL-53 (Al) is ~85 wt %, which tends to decrease as the Cr content increases. In air flow, as temperature increases from room temperature to 700 °C, all samples present *multistage* TG accompanied by corresponding exothermic DSC peaks due to combustion of organic contents. The corresponding derivative thermogravimetry (DTG) profiles are plotted in Figure S3. According to earlier studies, there are two groups of BDC species within the as-made MIL-53, namely, (i) BDCs coordinated to the metal nodes serving as the framework linkers and (ii) H_2BDC molecules confined within the microporosity of MIL-53 structures.[27,35] The presence of these two BDC species is mirrored by the combustion pathways, evidenced by the two-step release of

https://doi.org/10.1021/acs.jpcc.1c02623
J. Phys. Chem. C 2021, 125, 14039−14047

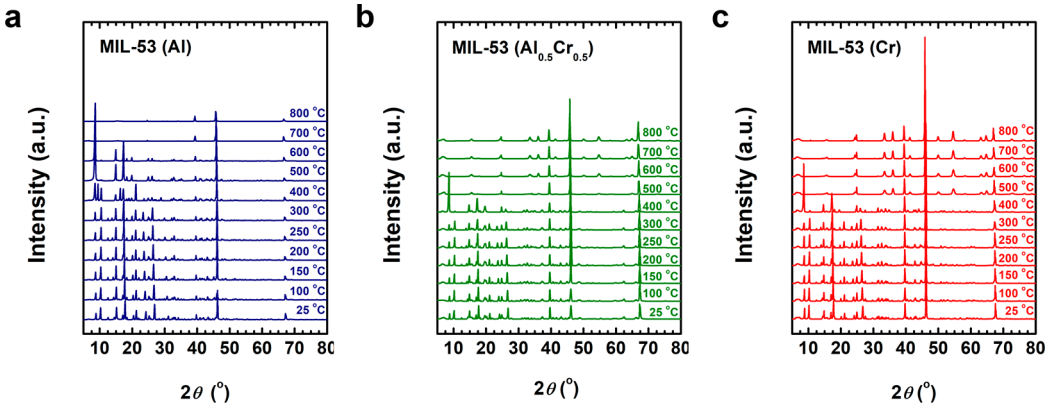

Figure 5. *In situ* X-ray diffraction (XRD) patterns of (a) MIL-53 (Al), (b) MIL-53 ($Al_{0.5}Cr_{0.5}$), and (c) MIL-53 (Cr) as a function of temperature in air flow (40 mL/min).

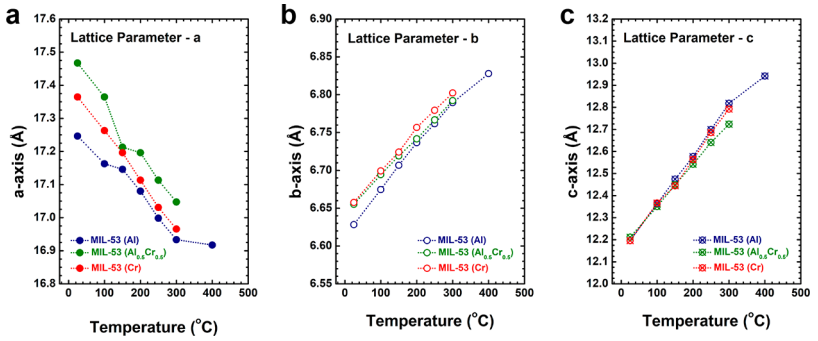

Figure 6. Lattice parameter evolutions of (a) MIL-53 (Al), (b) MIL-53 ($Al_{0.5}Cr_{0.5}$), and (c) MIL-53 (Cr) as a function of temperature in air flow (40 mL/min).

H_2O and CO_2 associated with consumption of O_2 in the air flow (see Figure 4b–d). Specifically, all MIL-53 ($Al_{1-x}Cr_x$) samples share a broad exothermic DSC peak centered at about 400 °C corresponding to the combustion of pore-confined H_2BDC molecules. This is supported by the broad peaks on the DSC and MS curves (m/z = 18, 32, and 44) within the same temperature range. On the other hand, as the Cr content increases, the oxidation temperature of coordinated BDC linkers systematically decreases, ranging from ∼550 °C for MIL-53 (Al) to ∼350 °C for MIL-53 (Cr) (see Figure 4d). Interestingly, in thermal analysis the combustion temperature of coordinated BDC appears to be lower than that of pore-confined BDC for MIL-53 (Cr).

Structural Stability of MIL-53 ($Al_{1-x}Cr_x$). The *in situ* XRD patterns of MIL-53 ($Al_{1-x}Cr_x$) reflecting the structural stability and evolution in air as a function of temperature are plotted in Figure 5. It has been found that the MIL-53 structure is highly dependent on the type and amount confined species within its pores.[53] As the temperature increases, the combustion of pore-confined H_2BDC molecules leads to a phase transition from a filled-pore *Pnma* phase to the empty pore phase of *Imma*, reported by Loiseau et al.[35] and observed at temperature above ∼300 °C in our structural analysis. Specifically, the transition from the *Pnma* to *Imma* phase is observed to conclude at ∼400 °C supported by thermal analysis results, which suggest complete combustion of pore-confined H_2BDC molecules (see Figure 4). Subsequently, at higher temperature, from 500 to 600 °C for MIL-53 (Al) and at about 400 °C for MIL-53 ($Al_{0.5}Cr_{0.5}$) and MIL-53 (Cr), the *Imma* phase is present. At above 600 °C for MIL-53 (Al), and 500 °C for MIL-53 ($Al_{0.5}Cr_{0.5}$) and MIL-53 (Cr) complete framework collapse occurs. The coordinated BDC linkers of MIL-53 ($Al_{1-x}Cr_x$) are decomposed and fully combusted to the final metal oxide products Al_2O_3 for MIL-53 (Al), Cr_2O_3 for MIL-53 (Cr), and a Al_2O_3/Cr_2O_3 mixed phase for MIL-53 ($Al_{0.5}Cr_{0.5}$). The additional peaks at above 600 °C for MIL-53 (Al) and 400 °C MIL-53 ($Al_{0.5}Cr_{0.5}$) and MIL-53 (Cr) are from the platinum (Pt) crucible, which hosts the samples during the *in situ* XRD experiments, as observed in our earlier studies.[31−34,54] Therefore, according to the *in situ* XRD results, we conclude that MIL-53 ($Al_{1-x}Cr_x$) present pore-filled *Pnma* structure up to initiation of phase transition estimated at ∼300 to 400 °C (see Figure 5) after removal of pore-confined H_2BDC molecules, followed by relatively stable pore-empty *Imma* structure up to ∼400 °C for MIL-53 (Cr) to higher than 500 °C for MIL-53 (Al), after which no MIL-53 pattern shows due to decomposition and combustion.

Lattice parameters of MIL-53 (Al), MIL-53 ($Al_{0.5}Cr_{0.5}$), and MIL-53 (Cr) as a function of temperature are presented in Figure 6. The unit cell volume changes are plotted in Figure 7. Crystallographic data for all samples are tabulated from room temperature *ex situ* and *in situ* XRD in Table 2 and Table S1, respectively. The *a*-parameter of each sample decreases near-linearly up to 300 °C, after which a phase transition from *Pnma* to *Imma* was observed on MIL-53 ($Al_{0.5}Cr_{0.5}$) and MIL-53 (Cr). The *a*-parameter of MIL-53 (Al) decreases less steeply from 300 to 400 °C as the phase transition to *Imma* occurs. Similar to this behavior, *b*- and *c*-parameters show near-linear increases up to 300 °C for all samples and less steep increases of MIL-53 (Al) up to 400 °C. Overall, as the temperature

https://doi.org/10.1021/acs.jpcc.1c02623
J. Phys. Chem. C 2021, 125, 14039−14047

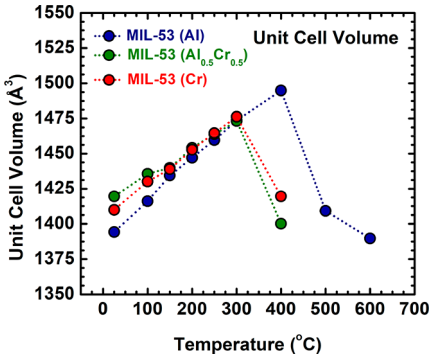

Figure 7. Unit cell volume changes of MIL-53 (Al), MIL-53 ($Al_{0.5}Cr_{0.5}$), and MIL-53 (Cr) as a function of temperature in air flow (40 mL/min). Both the unit cell volumes for *Pnma* and *Imma* phases are presented.

Table 2. Structural Parameters and Unit Cell Volume Calculated from X-ray Diffraction (XRD) Patterns for As-Synthesized MIL-53 Samples at Room Temperature

	Pnma			
sample	*a* (Å)	*b* (Å)	*c* (Å)	unit cell vol (Å^3)
MIL-53 (Al)[a]	17.25	6.63	12.20	1394
MIL-53 ($Al_{0.75}Cr_{0.25}$)[b]	17.59	6.68	12.24	1438
MIL-53 ($Al_{0.5}Cr_{0.5}$)[a]	17.47	6.66	12.21	1420
MIL-53 ($Al_{0.25}Cr_{0.75}$)[b]	17.54	6.67	12.27	1436
MIL-53 (Cr)[a]	17.36	6.66	12.20	1410

[a]Samples calculated by using *in situ* configuration in a platinum crucible. [b]Samples calculated in *ex situ* configuration on a glass slide. Such sample holder variation does not impact the structural parameters of the MIL-53 samples.

increases up to the point of phase transition from *Pnma* to *Imma*, the unit cell volume increases near-linearly with temperature (see Figure 7). Such variation of lattice parameters and unit cell volume is due to thermal expansion.[55] Following the expulsion of confined species observed in the TG-DSC-MS data and the concurrent phase transition to *Imma*, the unit cell volume decreases with temperature before structural degradation due to combustion. Generally, thermal structural evolution of Al-containing MIL-53 ($Al_{1-x}Cr_x$) can be distinguished into three stages: (i) *Pnma* thermal expansion, (ii) *Pnma* to *Imma* phase transition due to loss of confined H_2BDC species, and (iii) structural degradation of *Imma* with combustion of organic linkers and inorganic metals, in good agreement with the thermal events revealed in the thermal analysis using TG-DSC-MS under similar conditions. The differences observed in thermal analysis and *in situ* XRD studies, particularly in event temperatures, are likely due to the fact that an equilibrium time was applied in the *in situ* XRD experiments by holding the target temperature for 5 min prior to each scan, while the thermal analysis had a continuously evolving dynamic program with a fixed heating rate.

Thermodynamic Stability of MIL-53 ($Al_{1-x}Cr_x$). The enthalpies of formation (ΔH_f) derived from the measured enthalpies of combustion (ΔH_{com}) data of all as-synthesized MIL-53 ($Al_{1-x}Cr_x$) samples (*Pnma*) are plotted in Figure 8a as a function of Cr content. The thermodynamic cycle applied and thermochemical data experimentally collected from high-temperature drop combustion calorimetry measurements at 800 °C in O_2 flow are summarized in Table S2 and Table 3, respectively. Specifically, the ΔH_f of MIL-53 (Al) is 92.8 ± 73.4 kJ/mol. Considering the large molecular weight (MW) of MIL-53, this slightly positive value suggests that the as-synthesized MIL-53 (Al) is energetically less stable compared with the dense phase assemblage of Al_2O_3 and H_2BDC. However, substitution of Al by Cr in the MIL-53 framework stabilizes the system starting from the concentration of Cr at ~26 mol % where the formed bimetallic MIL-53 ($Al_{0.75}Cr_{0.25}$) has a significantly more negative enthalpy of formation, −693.9 ± 49.0 kJ/mol. Increasing the Cr content further enhances the thermodynamic stability of MIL-53 ($Al_{1-x}Cr_x$), which is reflected in the negative correlation between the Cr concentration and the ΔH_f of the corresponding MIL-53 sample (see Figure 8a). However, the enthalpic benefit from the substitution attenuates when Cr content is over the equimolar of Cr and Al, perhaps suggesting a nonlinear energetic impact from the random mixing of Cr and Al in the matrix. Specifically, the enthalpy of mixing (ΔH_{mix}) can be derived based on ΔH_f by using the methodology established previously.[56] Values of ΔH_{mix} shown in Figure 8b were fitted by the quadratic polynomial function, $\Omega \cdot x(1-x)$, where Ω = −2444.5 ± 239.2 kJ/mol represents the interaction parameter and x is the Cr concentration. The significantly negative value of Ω indicates that the mixing of Al and Cr within the MIL-53 lattice is strongly exothermic, which also explains the origins of thermodynamic stability due to the substitution of Al by Cr.

Therefore, although Cr introduction decreases both thermal and structural stability of MIL-53 ($Al_{1-x}Cr_x$), increased Cr

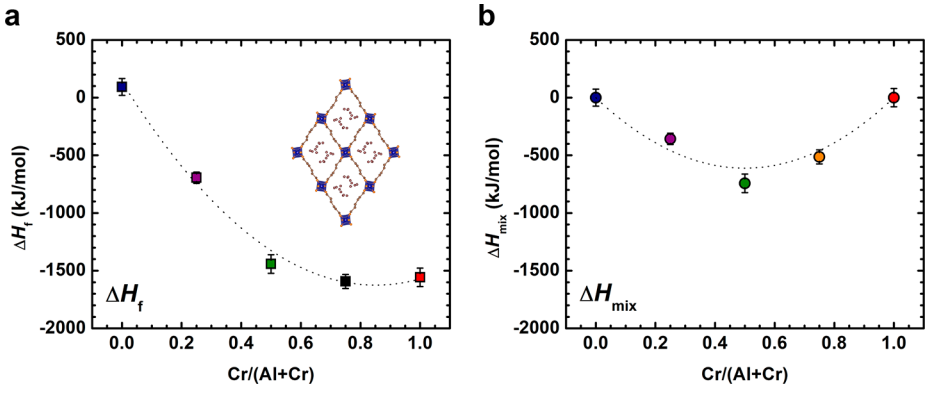

Figure 8. Enthalpies of (a) formation and (b) mixing for MIL-53 ($Al_{1-x}Cr_x$) (*Pnma* space group, x from 0 to 1) from corresponding crystalline dense metal oxides (Al_2O_3 or Cr_2O_3) and organic linker (H_2BDC) at 25 °C.

https://doi.org/10.1021/acs.jpcc.1c02623
J. Phys. Chem. C 2021, 125, 14039−14047

Table 3. Thermochemical Data from High-Temperature Drop Combustion Calorimetry Measurements at 800 °C in O_2 Flow

name	ΔH_{com} (kJ/mol MOF)	ΔH_r° (kJ/mol of metal)	$H_{800}^\circ - H_{25}^\circ$ (kJ/mol oxide)
MIL-53 (Al)	−4936.15 ± 70.20	92.84 ± 73.37	
MIL-53 ($Al_{0.75}Cr_{0.25}$)	−3920.82 ± 44.57	−693.85 ± 48.99	
MIL-53 ($Al_{0.5}Cr_{0.5}$)	−3543.15 ± 77.75	−1442.03 ± 80.79	
MIL-53 ($Al_{0.25}Cr_{0.75}$)	−2963.75 ± 57.34	−1593.15 ± 60.75	
MIL-53 (Cr)	−2685.04 ± 77.42	−1557.59 ± 79.65	
H_2BDC	−2852.76 ± 12.55		
Al_2O_3			91.22
Cr_2O_3			94.42
H_2O			78.45
CO_2			

content leads to enhanced energetic stability relevant to the dense phase assemblages of M_2O_3 (M = Al and Cr) and H_2BDC. In other words, and in a broader sense, most MOFs are thermodynamically favorable to be synthesized via fine-tuned compositional factors (metal and linker contents and solvents), yet the materials science and chemical engineering communities need to fully understand their properties within specific environmental limits to maximize their potential for industrial applications.

CONCLUSION

In this study, by use of TG-DSC-MS, *in situ* X-ray diffraction, and high-temperature drop combustion calorimetry, the thermal, structural, and energetic stabilities of MIL-53 ($Al_{1-x}Cr_x$) ($0 < x < 1$) in air were thoroughly investigated. This integrated stability evaluation suggests that Cr substitution weakens the thermal and structural stabilities for a particular MIL-53 ($Al_{1-x}Cr_x$) in air. Combustion of pore-confined H_2BDC molecules leads to a framework phase transition from *Pnma* to *Imma*, the empty-pore phase. Subsequently, structural degradation is associated with vigorous oxidation of the metal node-coordinated linkers. Eventually, complete oxidation results in formation of the inorganic Al_2O_3, Cr_2O_3, or their solid solution. On the other hand, the formation enthalpy of each MIL-53 ($Al_{1-x}Cr_x$) tends to be more exothermic from 92.8 ± 73.4 kJ/mol until reaching a plateau at about −1593.2 ± 60.8 kJ/mol as the Cr content increases. This suggests that MIL-53 (Al) is slightly metastable, while incorporation of Cr significantly stabilizes the framework. Such a phenomenon is very likely a product of enhanced H_2BDC−MIL-53 guest−host interactions as the Cr content increases, which energetically neutralizes the metastability of empty frameworks, as commonly seen in zeolite templated by using organic structural directing agents (OSDA). Different stability properties of MOFs, such as thermal, structural, and thermodynamic stabilities, share equal importance and need to be thoroughly evaluated prior to their applications in a specific industrial environment.

ASSOCIATED CONTENT

Supporting Information

The Supporting Information is available free of charge at https://pubs.acs.org/doi/10.1021/acs.jpcc.1c02623.

Additional XPS, DTG, and XRD data and thermochemical cycle (PDF)

AUTHOR INFORMATION

Corresponding Authors

Di Wu − *Alexandra Navrotsky Institute for Experimental Thermodynamics, The Gene and Linda Voiland School of Chemical Engineering and Bioengineering, Department of Chemistry, and Materials Science and Engineering, Washington State University, Pullman, Washington 99163, United States;* orcid.org/0000-0001-6879-321X; Email: d.wu@wsu.edu

Xiaofeng Guo − *Alexandra Navrotsky Institute for Experimental Thermodynamics, Department of Chemistry, and Materials Science and Engineering, Washington State University, Pullman, Washington 99163, United States;* orcid.org/0000-0003-3129-493X; Email: x.guo@wsu.edu

Authors

Esra Y. Mertsoy − *Alexandra Navrotsky Institute for Experimental Thermodynamics and The Gene and Linda Voiland School of Chemical Engineering and Bioengineering, Washington State University, Pullman, Washington 99163, United States; Department of Chemical Engineering, Ege University, Izumir 35100, Turkey*

Xianghui Zhang − *Alexandra Navrotsky Institute for Experimental Thermodynamics and The Gene and Linda Voiland School of Chemical Engineering and Bioengineering, Washington State University, Pullman, Washington 99163, United States*

Cody B. Cockreham − *Alexandra Navrotsky Institute for Experimental Thermodynamics and The Gene and Linda Voiland School of Chemical Engineering and Bioengineering, Washington State University, Pullman, Washington 99163, United States; Earth and Environmental Sciences Division, Los Alamos National Laboratory, Los Alamos, New Mexico 87545, United States*

Vitaliy G. Goncharov − *Alexandra Navrotsky Institute for Experimental Thermodynamics and Department of Chemistry, Washington State University, Pullman, Washington 99163, United States; Earth and Environmental Sciences Division, Los Alamos National Laboratory, Los Alamos, New Mexico 87545, United States*

Jun Wang − *Alexandra Navrotsky Institute for Experimental Thermodynamics and The Gene and Linda Voiland School of Chemical Engineering and Bioengineering, Washington State University, Pullman, Washington 99163, United States; School of Physics and Electronic Engineering, Sichuan University of Science and Engineering, Zigong, Sichuan 643036, China*

Nian Wei − *Alexandra Navrotsky Institute for Experimental Thermodynamics and Department of Chemistry, Washington State University, Pullman, Washington 99163, United States; College of Physics, Sichuan University, Chengdu, Sichuan 610064, China*

Hui Sun − *Petroleum Processing Research Center, School of Chemical Engineering and International Joint Research Center of Green Energy Chemical Engineering, East China University of Science and Technology, Shanghai 200237, China;* orcid.org/0000-0002-8544-756X

Complete contact information is available at: https://pubs.acs.org/10.1021/acs.jpcc.1c02623

Notes

The authors declare no competing financial interest.

■ ACKNOWLEDGMENTS

This work was supported by institutional funds from the Gene and Linda Voiland School of Chemical Engineering and Bioengineering and Alexandra Navrotsky Institute for Experimental Thermodynamics at Washington State University. X.Z. was supported by Chambroad Distinguished Scholarship. C.B.C. received support from the Achievement Rewards for College Scientists (ARCS) Fellowship from the ARCS Seattle Chapter. Part of this study was also supported by collaboration, services, and infrastructure through the Nuclear Science Center User Facility at WSU. H.S. acknowledges the funds from the National Natural Science Foundation of China (Grants 91634112 and 21878097) and the Natural Science Foundation of Shanghai (Grant 16ZR1408100).

■ REFERENCES

(1) Zhou, H. C.; Long, J. R.; Yaghi, O. M. Introduction to Metal-Organic Frameworks. *Chem. Rev.* **2012**, *112* (2), 673−674.

(2) Li, G.; Sun, H.; Xu, H.; Guo, X.; Wu, D. Probing the Energetics of Molecule-Material Interactions at Interfaces and in Nanopores. *J. Phys. Chem. C* **2017**, *121* (39), 26141−26154.

(3) Wu, D.; Guo, X.; Sun, H.; Navrotsky, A. Thermodynamics of Methane Adsorption on Copper HKUST-1 at Low Pressure. *J. Phys. Chem. Lett.* **2015**, *6* (13), 2439−2443.

(4) Lin, R.; Ge, L.; Liu, S.; Rudolph, V.; Zhu, Z. Mixed-Matrix Membranes with Metal-Organic Framework-Decorated CNT Fillers for Efficient CO_2 Separation. *ACS Appl. Mater. Interfaces* **2015**, *7* (27), 14750−14757.

(5) Wang, N.; Mundstock, A.; Liu, Y.; Huang, A.; Caro, J. Amine-Modified Mg-MOF-74/CPO-27-Mg Membrane with Enhanced H_2/CO_2 Separation. *Chem. Eng. Sci.* **2015**, *124*, 27−36.

(6) Sun, H.; Ren, D.; Kong, R.; Wang, D.; Jiang, H.; Tan, J.; Wu, D.; Chen, S.; Shen, B. Tuning 1-Hexene/n-Hexane Adsorption on MOF-74 via Constructing Co-Mg Bimetallic Frameworks. *Microporous Mesoporous Mater.* **2019**, *284*, 151−160.

(7) Sun, H.; Han, X.; Liu, K.; Shen, B.; Liu, J.; Wu, D.; Shi, X. Metal-Modified Cu-BTC Acid for Highly Enhanced Adsorption of Organosulfur Species. *Ind. Eng. Chem. Res.* **2017**, *56* (34), 9541−9550.

(8) Yılmaz, E.; Sert, E.; Atalay, F. S. Synthesis and Sulfation of Titanium Based Metal Organic Framework; MIL-125 and Usage as Catalyst in Esterification Reactions. *Catal. Commun.* **2017**, *100*, 48−51.

(9) Anılır, G.; Sert, E.; Yılmaz, E.; Atalay, F. S. Preparation and Performance of Functionalized Metal Organic Framework, MIL-101, for Knoevenagel Reaction. *J. Solid State Chem.* **2020**, *283*, 121138.

(10) Crake, A.; Christoforidis, K. C.; Kafizas, A.; Zafeiratos, S.; Petit, C. CO_2 Capture and Photocatalytic Reduction Using Bifunctional TiO_2/MOF Nanocomposites under UV−Vis Irradiation. *Appl. Catal., B* **2017**, *210*, 131−140.

(11) Yang, C.; You, X.; Cheng, J.; Zheng, H.; Chen, Y. A Novel Visible-Light-Driven In-Based MOF/Graphene Oxide Composite Photocatalyst with Enhanced Photocatalytic Activity toward the Degradation of Amoxicillin. *Appl. Catal., B* **2017**, *200*, 673−680.

(12) Chen, B.; Yang, Y.; Zapata, F.; Lin, G.; Qian, G.; Lobkovsky, E. B. Luminescent Open Metal Sites within a Metal-Organic Framework for Sensing Small Molecules. *Adv. Mater.* **2007**, *19* (13), 1693−1696.

(13) Gassensmith, J. J.; Kim, J. Y.; Holcroft, J. M.; Farha, O. K.; Stoddart, J. F.; Hupp, J. T.; Jeong, N. C. A Metal-Organic Framework-Based Material for Electrochemical Sensing of Carbon Dioxide. *J. Am. Chem. Soc.* **2014**, *136*, 8277−8282.

(14) Kreno, L. E.; Leong, K.; Farha, O. K.; Allendorf, M.; Van Duyne, R. P.; Hupp, J. T. Metal-Organic Framework Materials as Chemical Sensors. *Chem. Rev.* **2012**, *112* (2), 1105−1125.

(15) Hughes, J. T.; Navrotsky, A. MOF-5: Enthalpy of Formation and Energy Landscape of Porous Materials. *J. Am. Chem. Soc.* **2011**, *133* (24), 9184−9187.

(16) Hughes, J. T.; Bennett, T. D.; Cheetham, A. K.; Navrotsky, A. Thermochemistry of Zeolitic Imidazolate Frameworks of Varying Porosity. *J. Am. Chem. Soc.* **2013**, *135* (2), 598−601.

(17) Wu, D.; Gassensmith, J. J.; Gouvea, D.; Ushakov, S.; Stoddart, J. F.; Navrotsky, A. Direct Calorimetric Measurement of Enthalpy of Adsorption of Carbon Dioxide on CD-MOF-2, a Green Metal−Organic Framework. *J. Am. Chem. Soc.* **2013**, *135* (18), 6790−6793.

(18) Hughes, J. T.; Sava, D. F.; Nenoff, T. M.; Navrotsky, A. Thermochemical Evidence for Strong Iodine Chemisorption by ZIF-8. *J. Am. Chem. Soc.* **2013**, *135* (44), 16256−16259.

(19) Akimbekov, Z.; Katsenis, A. D.; Nagabhushana, G. P.; Ayoub, G.; Arhangelskis, M.; Morris, A. J.; Friscic, T.; Navrotsky, A. Experimental and Theoretical Evaluation of the Stability of True MOF Polymorphs Explains Their Mechanochemical Interconversions. *J. Am. Chem. Soc.* **2017**, *139* (23), 7952−7957.

(20) Novendra, N.; Marrett, J. M.; Katsenis, A. D.; Titi, H. M.; Arhangelskis, M.; Friscic, T.; Navrotsky, A. Linker Substituents Control the Thermodynamic Stability in Metal−Organic Frameworks. *J. Am. Chem. Soc.* **2020**, *142* (52), 21720−21729.

(21) Rosen, P. F.; Dickson, M. S.; Calvin, J. J.; Ross, N. L.; Friscic, T.; Navrotsky, A.; Woodfield, B. F. Thermodynamic Evidence of Structural Transformations in CO_2-Loaded Metal−Organic Framework $Zn(MeIm)_2$ from Heat Capacity Measurements. *J. Am. Chem. Soc.* **2020**, *142* (10), 4833−4841.

(22) Li, G.; Sun, H.; Xu, H.; Guo, X.; Wu, D. Probing the Energetics of Molecule-Material Interactions at Interfaces and in Nanopores. *J. Phys. Chem. C* **2017**, *121* (47), 26141−26154.

(23) Sun, H.; Wu, D. Recent Advances in Experimental Thermodynamics of Metal-Organic Frameworks. *Powder Diffr.* **2019**, *34*, 297.

(24) Wu, D.; Navrotsky, A. Thermodynamics of Metal−Organic Frameworks. *J. Solid State Chem.* **2015**, *223*, 53−58.

(25) Voskanyan, A. A.; Goncharov, V. G.; Novendra, N.; Guo, X.; Navrotsky, A. Thermodynamics Drives the Stability of the MOF-74 Family in Water. *ACS Omega* **2020**, *5* (22), 13158−13163.

(26) Rallapalli, P.; Patil, D.; Prasanth, K. P.; Somani, R. S.; Jasra, R. V.; Bajaj, H. C. An Alternative Activation Method for the Enhancement of Methane Storage Capacity of Nanoporous Aluminium Terephthalate, MIL-53(Al). *J. Porous Mater.* **2010**, *17* (5), 523−528.

(27) Serre, C.; Millange, F.; Thouvenot, C.; Noguès, M.; Marsolier, G.; Louër, D.; Férey, G. Very Large Breathing Effect in the First Nanoporous Chromium(III)-Based Solids: MIL-53 or CrIII(OH)·$\{O_2C\text{-}C_6H_4\text{-}\ CO_2\}$·$\{HO_2C\text{-}C_6H_4\ \text{-}CO_2H\}_x$·$H_2O_y$. *J. Am. Chem. Soc.* **2002**, *124* (45), 13519−13526.

(28) Khudozhitkov, A. E.; Toktarev, A. V.; Arzumanov, S. S.; Gabrienko, A. A.; Kolokolov, D. I.; Stepanov, A. G. Molecular Mobility of Tert-Butyl Alcohol Confined in a Breathing MIL-53 (Al) Metal-Organic Framework. *ChemPhysChem* **2020**, *21* (17), 1951−1956.

(29) Lieder, C.; Opelt, S.; Dyballa, M.; Henning, H.; Klemm, E.; Hunger, M. Adsorbate Effect on $AlO_4(OH)_2$ Centers in the Metal-Organic Framework MIL-53 Investigated by Solid-State NMR Spectroscopy. *J. Phys. Chem. C* **2010**, *114* (39), 16596−16602.
(30) Wang, J.; Yilmaz, E.; Zhang, X.; Li, H.; Zhang, R.; Guo, X.; Sun, H.; Wang, B.; Wu, D. Hydration Energetics of a Diamine-Appended Metal−Organic Framework Carbon Capture Sorbent. *J. Phys. Chem. C* **2020**, *124* (1), 398−403.
(31) Zhang, X.; Cockreham, C. B.; Yilmaz, E.; Li, G.; Li, N.; Ha, S.; Fu, L.; Qi, J.; Xu, H.; Wu, D. Energetic Cost for Being "Redox-Site-Rich" in Pseudocapacitive Energy Storage with Nickel − Aluminum Layered Double Hydroxide Materials. *J. Phys. Chem. Lett.* **2020**, *11* (9), 3745−3753.
(32) Zhang, X.; Cockreham, C. B.; Huang, Z.; Sun, H.; Yang, C.; Marin-Flores, O. G.; Wang, B.; Guo, X.; Ha, S.; Xu, H.; Wu, D. Thermodynamics of Water−Cationic Species−Framework Guest−Host Interactions within Transition Metal Ion-Exchanged Mordenite Relevant to Selective Anaerobic Oxidation of Methane to Methanol. *J. Phys. Chem. Lett.* **2020**, *11* (12), 4774−4784.
(33) Cockreham, C.; Zhang, X.; Goncharov, V.; Guo, X.; Xu, H.; Wu, D. Dehydration Pathway of $CoF_2{\cdot}4H_2O$ Revisited by Integrated Ex Situ and In Situ Calorimetric and Structural Studies. *J. Phys. Chem. C* **2020**, *124* (6), 3551−3556.
(34) Cockreham, C.; Zhang, X.; Li, H.; Hammond-Pereira, E.; Sun, J.; Saunders, S. R.; Wang, Y.; Xu, H.; Wu, D. Inhibition of $AlF_3{\cdot}3H_2O$ Impurity Formation in $Ti_3C_2T_x$ MXene Synthesis under a Unique CoF_x/HCl Etching Environment. *ACS Appl. Energy Mater.* **2019**, *2* (11), 8145−8152.
(35) Loiseau, T.; Serre, C.; Huguenard, C.; Fink, G.; Taulelle, F.; Henry, M.; Bataille, T.; Férey, G. A Rationale for the Large Breathing of the Porous Aluminum Terephthalate (MIL-53) Upon Hydration. *Chem. - Eur. J.* **2004**, *10* (6), 1373−1382.
(36) Guo, X.; Boukhalfa, H.; Mitchell, J. N.; Ramos, M.; Gaunt, A. J.; Migliori, A.; Roback, R. C.; Navrotsky, A.; Xu, H. Sample Seal-and-Drop Device and Methodology for High Temperature Oxide Melt Solution Calorimetric Measurements of PuO_2. *Rev. Sci. Instrum.* **2019**, *90* (4), 044101.
(37) Millange, F.; Serre, C.; Férey, G. Synthesis, Structure Determination and Properties of MIL-53as and MIL-53ht: The First CrIII Hybrid Inorganic-Organic Microporous Solids: CrIII-$(OH){\cdot}(O_2C\text{-}C_6H_4\text{-}CO_2){\cdot}(HO_2C\text{-}C_6H_4\text{-}CO_2H)_x$. *Chem. Commun.* **2002**, *8*, 822−823.
(38) Moran, C. M.; Joshi, J. N.; Marti, R. M.; Hayes, S. E.; Walton, K. S. Structured Growth of Metal-Organic Framework MIL-53(Al) from Solid Aluminum Carbide Precursor. *J. Am. Chem. Soc.* **2018**, *140* (29), 9148−9153.
(39) Serre, C.; Millange, F.; Thouvenot, C.; Noguès, M.; Marsolier, G.; Louër, D.; Férey, G. Very Large Breathing Effect in the First Nanoporous Chromium(III)-Based Solids: MIL-53 or $Cr^{III}(OH){\cdot}\{O_2C\text{−}C_6H_4\text{−}CO_2\}{\cdot}\{HO_2C\text{−}C_6H_4\text{−}CO_2H\}_x{\cdot}H_2O_y$. *J. Am. Chem. Soc.* **2002**, *124* (45), 13519−13526.
(40) Do, X.-D.; Hoang, V.-T.; Kaliaguine, S. MIL-53 (Al) Mesostructured Metal-Organic Frameworks. *Microporous Mesoporous Mater.* **2011**, *141* (1−3), 135−139.
(41) Nouar, F.; Devic, T.; Chevreau, H.; Guillou, N.; Gibson, E.; Clet, G.; Daturi, M.; Vimont, A.; Greneche, J. M.; Breeze, M. I.; Walton, R. I.; Llewellyn, P. L.; Serre, C.; et al. Tuning the Breathing Behaviour of MIL-53 by Cation Mixing. *Chem. Commun.* **2012**, *48*, 10237−10239.
(42) Li, C.; Xiong, Z.; Zhang, J.; Wu, C. The Strengthening Role of the Amino Group in Metal-Organic Framework MIL-53 (Al) for Methylene Blue and Malachite Green Dye Adsorption. *J. Chem. Eng. Data* **2015**, *60* (11), 3414−3422.
(43) Warfsmann, J.; Tokay, B.; Champness, N. R. Synthesis of Hydrophobic MIL-53(Al) Nanoparticles in Low Molecular Weight Alcohols: Systematic Investigation of Solvent Effects. *CrystEngComm* **2018**, *20* (32), 4666−4675.
(44) Khan, N. A.; Jhung, S. H. Phase-Transition and Phase-Selective Synthesis of Porous Chromium-Benzenedicarboxylates. *Cryst. Growth Des.* **2010**, *10* (4), 1860−1865.
(45) Leng, K.; Sun, Y.; Li, X.; Sun, S.; Xu, W. Rapid Synthesis of Metal-Organic Frameworks MIL-101(Cr) Without the Addition of Solvent and Hydrofluoric Acid. *Cryst. Growth Des.* **2016**, *16* (3), 1168−1171.
(46) Rallapalli, P. B. S.; Raj, M. C.; Senthilkumar, S.; Somani, R. S.; Bajaj, H. C. HF-Free Synthesis of MIL-101(Cr) and Its Hydrogen Adsorption Studies. *Environ. Prog. Sustainable Energy* **2016**, *35* (1), 461−468.
(47) Nguyen, V. H.; Nguyen, T. D.; Bach, L. G.; Hoang, T.; Bui, Q. T. P.; Tran, L. D.; Nguyen, C. V.; Vo, D. V. N.; Do, S. T. Effective Photocatalytic Activity of Mixed Ni/Fe-Base Metal-Organic Framework under a Compact Fluorescent Daylight Lamp. *Catalysts* **2018**, *8* (11), 487.
(48) Tanasaro, T.; Adpakpang, K.; Ittisanronnachai, S.; Faungnawakij, K.; Butburee, T.; Wannapaiboon, S.; Ogawa, M.; Bureekaew, S. Control of Polymorphism of Metal-Organic Frameworks Using Mixed-Metal Approach. *Cryst. Growth Des.* **2018**, *18* (1), 16−21.
(49) Sun, H.; Ren, D.; Kong, R.; Wang, D.; Jiang, H.; Tan, J.; Wu, D.; Chen, S.; Shen, B. Tuning 1-Hexene/n-Hexane Adsorption on MOF-74 via Constructing Co-Mg Bimetallic Frameworks. *Microporous Mesoporous Mater.* **2019**, *284*, 151−160.
(50) Lu, T.; Song, H.; Dong, X.; Hu, J.; Lv, Y. A Highly Selective and Fast-Response Photoluminescence Humidity Sensor Based on F^- Decorated NH_2-MIL-53(Al) Nanorods. *J. Mater. Chem. C* **2017**, *5*, 9465−9471.
(51) Guo, H.; Wang, D.; Chen, J.; Weng, W.; Huang, M.; Zheng, Z. Simple Fabrication of Flake-like NH_2 -MIL-53 (Cr) and Its Application as an Electrochemical Sensor for the Detection of Pb^{2+}. *Chem. Eng. J.* **2016**, *289*, 479−485.
(52) Yang, K.; Zhou, L.; Yu, G.; Xiong, X.; Ye, M.; Li, Y.; Lu, D.; Pan, Y.; Chen, M.; Zhang, L.; et al. Ru Nanoparticles Supported on MIL-53(Cr, Al) as Efficient Catalysts for Hydrogen Generation from Hydrolysis of Ammonia Norane. *Int. J. Hydrogen Energy* **2016**, *1*, 0−9.
(53) Mounfield, W. P.; Walton, K. S. Effect of Synthesis Solvent on the Breathing Behavior of MIL-53(Al). *J. Colloid Interface Sci.* **2015**, *447*, 33−39.
(54) Cockreham, C. B.; Zhang, X.; Lau, M. L.; Long, M.; Guo, X.; Xu, H.; Wu, D. Thermal Evolutions and Resulting Microstructural Changes in Kerogen-Rich Marcellus Shale. *ACS Earth Space Chem.* **2020**, *4* (12), 2461−2469.
(55) Nanthamathee, C.; Ling, S.; Slater, B.; Attfield, M. P. Contradistinct Thermoresponsive Behavior of Isostructural MIL-53 Type Metal-Organic Frameworks by Modifying the Framework Inorganic Anion. *Chem. Mater.* **2015**, *27* (1), 85−95.
(56) Guo, X.; Szenknect, S.; Mesbah, A.; Clavier, N.; Poinssot, C.; Wu, D.; Xu, H.; Dacheux, N.; Ewing, R.; Navrotsky, A. Energetics of a Uranothorite $(Th_{1-x}U_xSiO_4)$ Solid Solution. *Chem. Mater.* **2016**, *28* (19), 7117−7124.

https://doi.org/10.1021/acs.jpcc.1c02623
J. Phys. Chem. C 2021, 125, 14039−14047